

Ammonium CI-Orbitrap: a tool for characterizing the reactivity of oxygenated organic molecules

Dandan Li¹, Dongyu Wang², Lucia Caudillo³, Wiebke Scholz⁴, Mingyi Wang^{5,6}, Sophie Tomaz¹, Guillaume Marie³, Mihnea Surdu², Elias Eccli⁴, Xianda Gong⁷, Loic Gonzalez-Carracedo⁸, Manuel Granzin³, Joschka Pfeifer^{3,9}, Birte Rörup¹⁰, Benjamin Schulze⁶, Pekka Rantala¹⁰, Sébastien Perrier¹, Armin Hansel⁴, Joachim Curtius³, Jasper Kirkby^{3,9}, Neil M. Donahue⁵, Christian George¹, Imad El-Haddad², Matthieu Riva^{1,*}

¹ Univ Lyon, Université Claude Bernard Lyon 1, CNRS, IRCELYON, 69626, Villeurbanne, France

⁶ Institute for Atmospheric and Earth System Research/Physics, Faculty of Science, University of Helsinki, 00014, Helsinki, Finland

² Laboratory of Atmospheric Chemistry, Paul Scherrer Institute, 5232, Villigen, Switzerland

³ Institute for Atmospheric and Environmental Sciences, Goethe University Frankfurt, 60438, Frankfurt am Main, Germany

⁴ Institute for Ion Physics and Applied Physics, University of Innsbruck, 6020, Innsbruck, Austria

⁵ Center for Atmospheric Particle Studies, Carnegie Mellon University, Pittsburgh, PA, 15213, USA

⁶ now at Division of Chemistry and Chemical Engineering, California Institute of Technology, Pasadena, CA 91125, USA

⁷ Leibniz Institute for Tropospheric Research, 04318, Leipzig, Germany

⁸ Faculty of Physics, University of Vienna, Vienna, 1090, Austria

⁹ CERN, the European Organization for Nuclear Research, CH-1211 Geneve 23, Switzerland

¹⁰ Institute for Atmospheric and Earth System Research/Physics, Faculty of Science, University of Helsinki, 00014, Helsinki, Finland

* Email: matthieu.riva@ircelyon.univ-lyon1.fr

25 Abstract

26 Oxygenated organic molecules (OOMs) play an important role in the formation of atmospheric
27 aerosols. Due to various analytical challenges in measuring organic vapors, uncertainties remain in the
28 formation and fate of OOMs. The chemical ionization Orbitrap mass spectrometer (CI-Orbitrap) has
29 recently been shown to be a powerful technique able to accurately identify gaseous organic
30 compounds due to its great mass resolving power. Here we present the ammonium ion (NH_4^+) based
31 CI-Orbitrap as a technique capable of measuring a wide range of gaseous OOMs. The performance of
32 the NH_4^+ -Orbitrap was compared with that of state-of-the-art mass spectrometers, including a nitrate
33 ion (NO_3^-) based CI coupled to an atmospheric pressure interfaced to long time-of-flight mass
34 spectrometer (APi-LTOF), a new generation of proton transfer reaction-TOF mass spectrometer
35 (PTR3-TOF), and an iodide (I^-) based CI-TOF mass spectrometer equipped with a Filter Inlet for
36 Gases and AEROSols (FIGAERO-CIMS). The instruments were deployed simultaneously in the
37 Cosmic Leaving OUtdoors Droplets (CLOUD) chamber at the European Organization for Nuclear
38 Research (CERN) during the CLOUD14 campaign in 2019. Products generated from α -pinene
39 ozonolysis across multiple experimental conditions were simultaneously measured by the mass
40 spectrometers. NH_4^+ -Orbitrap was able to identify the widest range of OOMs (i.e., $\text{O} \geq 2$), from low
41 oxidized species to highly oxygenated organic molecules (HOMs). Excellent agreements were found
42 between the NH_4^+ -Orbitrap and the NO_3^- -LTOF for characterizing HOMs and with the PTR3-TOF for
43 the less oxidized monomeric species. A semi-quantitative information was retrieved for OOMs
44 measured by NH_4^+ -Orbitrap using calibration factors derived from this side-by-side comparison. As
45 other mass spectrometry techniques used during this campaign, the detection sensitivity of NH_4^+ -
46 Orbitrap to OOMs is greatly affected by relative humidity, which may be related to changes in
47 ionization efficiency and/or multiphase chemistry. Overall, this study shows that NH_4^+ ion-based
48 chemistry associated with the high mass resolving power of the Orbitrap mass analyzer can measure
49 almost all-inclusive compounds. As a result, it is now possible to cover the entire range of compounds,
50 which can lead to a better understanding of the oxidation processes.

51

52 **1 Introduction**

53 Aerosols affect the climate by either directly scattering or absorbing solar radiation, or acting as seeds
54 for cloud formation (Fan et al., 2016; Haywood and Boucher, 2000). A major fraction of submicron
55 aerosol mass consists of organic compounds, with secondary organic aerosol (SOA) predominating
56 (Jimenez et al., 2009; Hallquist et al., 2009). Oxygenated organic molecules (OOMs) generated from
57 the oxidation of volatile organic compounds (VOCs) contribute to the formation and growth of SOA
58 (Ehn et al., 2014; Mellouki et al., 2015). **OOMs can be generated through bimolecular peroxy radicals
59 (RO_2) pathway or by the autoxidation of RO_2 followed by the termination pathways (Bianchi et al.,
60 2019; Mohr et al., 2019).** Among the OOMs, the highly oxygenated organic molecules (HOMs),
61 containing multiple functional groups and exhibiting (extremely) low saturation vapor pressure, can
62 nucleate in concert with inorganic species e.g., sulfuric acid or on their own (Ehn et al., 2014; Kirkby
63 et al., 2016; Bianchi et al., 2016), forming new particles. Less oxygenated molecules (i.e., containing 2
64 to 5 oxygen atoms) play a vital role in the growth of newly formed atmospheric particles, either by
65 condensation or through multiphase chemistry (Bianchi et al., 2019; Ehn et al., 2014; Hallquist et al.,
66 2009). Therefore, the identification and quantification of the wide diversity of OOMs are essential to
67 understand SOA formation and growth (Kirkby et al., 2016; Bianchi et al., 2016; Ehn et al., 2014).

68 Mass spectrometry (MS) has made remarkable achievements in detecting, characterizing, and
69 quantifying OOMs (Wang et al., 2020; Breitenlechner et al., 2017; Bianchi et al., 2019; Ehn et al.,
70 2010; Riva et al., 2019a). Moreover, the application of chemical ionization (CI) enables the detection
71 of a wide variety of organic and inorganic analytes (Bianchi et al., 2019; Ehn et al., 2014; Jokinen et
72 al., 2012; Lee et al., 2014). However, the selection of ionization chemistry in combination with MS
73 detection technique will impact the methods selectivity and sensitivity toward certain groups of OOMs
74 (Bianchi et al., 2019; Riva et al., 2020; Riva et al., 2019b; Berndt et al., 2018b; Berndt et al., 2018a).
75 **For example, negative ion-based chemistry, including nitrate (NO_3^-), can optimally detect HOMs,
76 which only constitute a small subset of the OOMs (Lee et al., 2014; Berndt et al., 2018b; Riva et al.,
77 2019b); iodide (I^-) can efficiently detect various OOMs with 3-5 oxygen atoms (Riva et al., 2019b;
78 Lee et al., 2014).** Positive ion-based chemistries have also been developed, showing great sensitivity to
79 HOMs as well as less oxidized products, providing the possibility of achieving carbon closure of the
80 OOMs (Berndt et al., 2018a; Berndt et al., 2018b; Hansel et al., 2018; Riva et al., 2020; Riva et al.,
81 2019b). However, these positive ion methods are mainly based on proton transfer and often result in
82 fragmentation of the analytes (Breitenlechner et al., 2017). Time-of-flight (TOF) mass spectrometers
83 using ammonium (NH_4^+) or amines as reagent ions can detect a wide variety of OOMs but suffer from
84 a lack of mass resolving power, making peak identification challenging, especially for complex
85 systems, i.e., under ambient conditions (Berndt et al., 2018b; Berndt et al., 2018a; Riva et al., 2019b).
86 Finally, the recently developed Orbitrap mass spectrometer using propylamine has achieved
87 unambiguous identification of overlapping peaks and accurate quantification of OOMs (Riva et al.,
88 2020). However, this analytical technique has been used in very diluted and dry environments to
89 ensure a linear response to the OOMs produced from simple atmospheric systems, i.e., a single VOC
90 precursor and oxidant (Riva et al., 2020; Riva et al., 2019b).

91 Here, we explore the capability of NH_4^+ ion-based CI-Orbitrap mass spectrometer (Q-Exactive
92 Orbitrap, Thermo Scientific) for detecting OOMs generated from α -pinene ozonolysis in the Cosmic
93 Leaving OUtdoors Droplets (CLOUD) chamber at the European Organization for Nuclear Research
94 (CERN) under various environmental conditions. We compare the performance of the NH_4^+ -Orbitrap
95 to state-of-the-art online mass spectrometers including a nitrate CI atmospheric pressure interface long
96 time of flight mass spectrometer (NO_3^- -LTOF; Tofwerk AG), a proton transfer reaction time of flight
97 mass spectrometer (PTR3-TOF; Ionicon Analytik GmbH), and gas phase of an iodide CI time of flight
98 mass spectrometer equipped with a Filter Inlet for Gases and AEROSols (I^- -CIMS, Tofwerk AG).

99 **2 Experimental approach and product analysis**

100 **2.1 CLOUD chamber experiments**

101 All experiments were conducted in the CLOUD chamber, a 26 m³ cylindrical stainless-steel vessel at
102 CERN. The chamber can achieve a pristine background for the study of nucleation (Kirkby et al.,
103 2016). The chamber operated as a continuously stirred tank reactor (CSTR), with mixing driven by
104 two inductively coupled fans at the top and bottom of the chamber. Evaporated liquid nitrogen (N_2)
105 and liquid oxygen (O_2) were blended at a ratio of 79:21 to provide ultra-pure synthetic air, which
106 flushed the chamber constantly. Variable amounts of trace gases, including O_3 , VOCs, NO_x , SO_2 , and
107 CO were accurately injected into the chamber via a gas control system and monitored. Photolysis was
108 driven by various light sources, including Hg-Xe UV lamps, and UV excimer laser. Between
109 experiments, the chamber was cleaned by irrigating the walls with ultra-pure water, then heated to 373
110 K, and flushed with humidified pure air and high ozone, reducing the contaminant (e.g., VOCs) to sub
111 pptv levels. During the cleaning process, particles were removed using a high-voltage electric field.

112 The results presented here were from the CLOUD14 campaign performed in autumn 2019.
113 During CLOUD14, the total flow was kept at 250 standard liters per minute (slpm), providing an
114 average residence time of 104 minutes. α -Pinene was introduced into the chamber by passing a small
115 flow of dry air over a temperature-controlled evaporator containing liquid α -pinene. Ozone was
116 generated by flowing a small fraction of the air through a quartz tube surrounded by UVC lights
117 (wavelength < 240 nm). Experiments were performed at low temperature (263 ± 0.1 K). The RH in the
118 chamber was controlled by flowing a portion of the air through a Nafion® humidifier using ultrapure
119 water (18 M Ω cm, Millipore Corporation). The contents of the chamber were monitored by a wide
120 range of external instruments connected to the sampling probes that protrude ~1 m into the chamber.

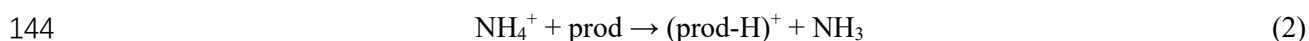
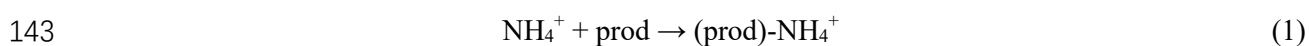
121 **2.2 Product analysis by NH_4^+ -Orbitrap**

122 The chemical composition of closed-shell molecules was determined in real time by means of a CI-
123 Orbitrap sampling from the CLOUD chamber through a 750 mm long, 10 mm inner diameter Teflon
124 tube at a flow rate of 10 slpm. The CI inlet mounted on the Orbitrap was custom-built with minor
125 modifications from the commercial inlet (Riva et al., 2019a). The ion-molecule reaction (IMR)
126 proceeded at atmospheric pressure with a residence time of 200-300 ms. The same operating
127 parameters used in our previous studies (RF level 60, automatic gain control 1×10^6 charges,

128 maximum injection time 1000 ms, multi RF ratio 1.2, mass resolution $m/\Delta m$ 140,000 at m/z 200),
129 were used, thereby minimizing declustering and maximizing the linearity range (Riva et al., 2019a;
130 Riva et al., 2020; Cai et al., 2022).

131 The high resolution Orbitrap mass spectra data were analyzed using “Orbitool” software with a
132 graphical user interface (GUI) (<https://orbitrap.catalyse.cnrs.fr>) (Cai et al., 2021). The analysis
133 procedures included data averaging, noise determination and reduction, single peak fitting, mass
134 calibration, assignment of molecular formulas, and export of time series. Signals were averaged over
135 5 min before determining the noise and performing mass calibration.

136 NH_4^+ has been utilized in PTR-MS with a low pressure (Berndt et al., 2018b; Hansel et al., 2018).
137 Here, this ionization technique was used to detect OOMs in atmospheric pressure and was operated in
138 a similar fashion as in our initial study (Riva et al., 2019a). NH_3 was added into the ion source by
139 flushing 2 sccm of dry air over the headspace of a 1% liquid ammonia water mixture (prepared from a
140 MilliQ water and a 25% ammonium hydroxide stock solution, ACS reagent, Sigma-Aldrich). The
141 product molecules (“prod”) were softly charged by binding to ammonium (NH_4^+) ions, forming
142 (prod)- NH_4^+ adduct ions or protonated products (prod)- H^+ , following either reaction (1) or (2),



145 The NH_4^+ reagent ion cannot be directly detected due to the cut-off of the Orbitrap mass analyzer
146 (i.e, m/Q 50). Hence, normalization of the raw analyte signals is difficult and hinders quantification of
147 OOMs. However, we observed a total of 62 peaks corresponding to amines, including $\text{C}_4\text{H}_{12}\text{N}^+$, and
148 $\text{C}_6\text{H}_{14}\text{N}^+$, which are formally ammonia derivatives. To some extent, their signals can be used to
149 correct for changes in NH_4^+ ion chemistry. Among these peaks, 13 were abundant and constant
150 throughout the measurement period (Fig. S1). As a result, these signals were used as surrogates for
151 the primary reagent ions to normalize the signal intensity of the OOMs (equation 3) and to account for
152 the potential variation of the ionization process (Riva et al., 2019b).

$$153 \quad [\text{OOM}]_{\text{nor}} = \frac{[(\text{OOM})\text{-NH}_4^+] + [(\text{OOM}\text{-H})^+]}{\Sigma[\text{Amine}]} \quad (3)$$

154 No direct calibration has been performed for the NH_4^+ -Orbitrap, but a semi-quantitative method
155 was used to estimate the OOMs concentrations based on the correlation analysis using the NO_3^- -
156 LTOF or the PTR3-TOF. The values of the Pearson correlation coefficients (R^2) were determined
157 between the NH_4^+ -Orbitrap and two other instruments using the timeseries during two runs (run 2211
158 and 2213). This includes AP injection, steady state stage, NO_x or CO injections, and RH variation. As
159 a result, for one compound, 755 data points were recorded and used for the correlation analysis. For
160 each instrument (referred to as *REF*), OOMs with R^2 greater than 0.9 (i.e., A) between *REF* and NH_4^+ -
161 Orbitrap, were used to determine a calibration factor ($c_{\text{Orbi-REF}}$, molecules cm^{-3}) and retrieve the
162 concentrations of OOMs measured by the NH_4^+ -Orbitrap according to the following equations 4-5:

163
$$c_{Orbi-REF} = \frac{[A]_{REF}}{[A]_{nor}} \quad (4)$$

164
$$[OOM]_{Orbi-REF} = c_{Orbi-REF} \times [OOM]_{nor} \quad (5)$$

165 The calibration factor between the NH_4^+ -Orbitrap and REF ($\sim 2.62 \times 10^8$ for NO_3^- -LTOF and $\sim 4.83 \times$
166 10^8 for PTR3-TOF) was assumed to be constant for all the OOMs. However, decomposition of
167 peroxides (i.e., ROOR and ROOH) can be expected within the PTR3-TOF. While fragmentation of
168 dimeric compounds can contribute to the overall signal of the monomers, the concentration of such
169 species remains minor (Li et al., 2022). As a result, we do not expect large enhancement of the
170 monomers signal intensity. Finally, a temperature-dependent sampling-line loss correction factor was
171 applied (Simon et al., 2020).

172 2.3 Product analysis by NO_3^- -LTOF

173 Detection of RO_2 radicals and closed-shell products was also performed by the NO_3^- -LTOF which has
174 been described elsewhere (Jokinen et al., 2012; Caudillo et al., 2021). Therefore, only relevant details
175 for this study are provided here. The NO_3^- -LTOF used in this study had a mass resolving power of
176 $m/\Delta m$ 12,000 and detected OOMs (mass 300-650 Da) as clusters ions with $(\text{HNO}_3)_n(\text{NO}_3^-)$ anions,
177 with $n = 0-2$. The limit of detection (LoD) for OOMs is 5×10^4 molecules cm^{-3} (Simon et al., 2020).
178 The primary ions were produced by a corona discharge needle exposed to a sheath gas enriched by
179 HNO_3 . Laminar flow diffusional loss was assumed in the 30 cm sampling line. A core-sampling
180 technique was applied, which drew a core flow of 5.1 slpm from the center of a 30 slpm total flow.
181 This setup reduced the sampling loss rate of HOMs to less than 30% (Simon et al., 2020).

182 The data were processed using Tofware (Version 3.2, Aerodyne Inc., USA) and MATLAB
183 R2019b (MathWorks, Inc., USA). In addition, background signals, mass-dependent transmission
184 efficiency (Heinritzi et al., 2016), and sampling losses (Simon et al., 2020) were determined and
185 corrections were applied. The NO_3^- -LTOF was directly calibrated using sulfuric acid (H_2SO_4), where
186 the detection efficiency of HOMs was assumed as similar to H_2SO_4 . However, OOMs with less
187 oxygen number ($\text{O} < 6$) were prone to a lower detection efficiency compared to H_2SO_4 , leading to an
188 underestimation (Stolzenburg et al., 2018; Ehn et al., 2014). A calibration factor C was determined to
189 be $\sim 4.13 \times 10^{10}$ molecules cm^{-3} during CLOUD14 (Caudillo et al., 2021). The concentration of OOMs
190 was also corrected using a mass dependent transmission efficiency inferred by depleting the reagent
191 ions with several perfluorinated acids. Assuming that OOMs got lost in sampling lines due to
192 diffusion, the losses of OOMs were corrected with a diffusion coefficient scaling with the molecular
193 mass. More information could be found in former studies (Heinritzi et al., 2016; Stolzenburg et al.,
194 2018; Simon et al., 2020; Caudillo et al., 2021).

195 2.4 Product analysis by PTR3-TOF

196 The PTR3-TOF ionizes organic compounds by proton transfer or ligand switch reactions where
197 protonated water clusters $(\text{H}_2\text{O})_n\text{H}_3\text{O}^+$ with $n=1-3$ were produced by a corona discharge using
198 humidified nitrogen (Breitenlechner et al., 2017). To reduce sample losses, a 2 slpm was drawn from a

199 10 slpm laminar flow through a critical orifice into the tripole where the ion-molecule reactions occur.
200 The pressure in this region was maintained at ~80 mbar. The distribution of primary ions and sample
201 molecules can be adjusted by a tunable radio frequency signal applied to the tripole rods. The LoD of
202 PTR3-TOF for detecting OOMs is 8×10^5 molecules cm^{-3} (Breitenlechner et al., 2017).

203 During the CLOUD14 experiments, the collision energy was controlled between 62 and 72 Td to
204 reduce the methods humidity dependence which may complicate the detection of organic compounds.
205 A gas standard mixture containing 1 ppm of 3-hexanone, heptanone, and α -pinene in nitrogen was
206 dynamically diluted by a factor of 1000 in VOC-free air to contain 1 ppbv of each compound, and
207 then was used to calibrate the PTR3-TOF. All data were analyzed using TOF-Tracer software running
208 on Julia 0.6 (<https://github.com/lukasfischer83/TOF-Tracer>) and were further corrected for the duty
209 cycle transmission of TOF and temperature dependent sampling line losses (Stolzenburg et al., 2018).
210 On the one hand, duty cycle corrected counts per second dcps, $\text{dcps}_i = \text{cps}_i \times (101/m_i)^{1/2}$, was utilized
211 to account for the mass-dependent transmission of the TOF mass spectrometer (Breitenlechner et al.,
212 2017). The calculated sensitivities of 3-hexanone and heptanone were comparable to the observed
213 ones. Therefore, the concentration of oxygenated products was estimated using the sensitivity of 3-
214 hexanone as lower-limit values due to possible fragmentation (Breitenlechner et al., 2017;
215 Stolzenburg et al., 2018). On the other hand, the detected OOMs having (extremely) low volatility
216 were assumed to be lost by diffusion and adjusted by a temperature dependent loss-correction. The
217 sampling line losses considered three loss sections under different temperatures, including losses at
218 the sampling lines within and outside the chamber and within the PTR3-TOF instrument. Details can
219 be found in previous studies (Breitenlechner et al., 2017; Stolzenburg et al., 2018).

220 **2.5 Product analysis by Γ -CIMS**

221 The Γ -CIMS was capable of characterizing both gas and particle phases (Lopez-Hilfiker et al., 2014).
222 In the gas-phase mode, gases were directly sampled into a 100-mbar turbulent ion-molecule reactor,
223 while particles were collected onto a polytetrafluoroethylene (PTFE) filter through a separate
224 dedicated sampling port. Analytes were then ionized with Γ chemical ionization and extracted into a
225 TOF mass analyzer (Wang et al., 2020). The LoD of Γ -CIMS for OOMs could be lower to $\sim 10^7$
226 molecules cm^{-3} (Lee et al., 2014). In this study, only gas phase data are reported.

227 Iodide ions (Γ) were used as the reagent ions and formed by passing a 1.0 slpm flow of ultrahigh
228 purity N_2 over a diffusion tube filled with methyl iodide (CH_3I), and then through a ^{210}Po radioactive
229 source. In the sampling mode, the reagent ion flow was mixed with a sample flow in the IMR at ~150
230 mbar. Coaxial core sampling was used to minimize the vapor wall loss in the sampling line. The total
231 flow was kept at 18.0 slpm and the core flow at 4.5 slpm; the instrument sampled at the center of the
232 core flow with a flow rate of 1.6 slpm. The gas-phase background signal was determined by routinely
233 introducing zero air directly into the inlet. Data were analyzed using Tofware (2.5.11_FIGAERO
234 version; Aerodyne Inc., USA) giving 10 s average mass spectra. The ion signal was normalized by the
235 sum of reagent ion signals (i.e., m/Q 127: Γ and 145: H_2OI).

236 2.6 Volatility of OOMs

237 It is challenging to directly measure the vapor pressure of individual OOMs due to the difficulty to
238 acquire authentic standards. To overcome experimental challenges, model calculations have been
239 developed to estimate the vapor pressure using, for example, structure-based estimations and formula-
240 based estimations (Pankow and Asher, 2008). Volatility basis set (VBS), a categorization framework
241 based on quantifiable organic property (i.e., volatility) has been established and is frequently used to
242 characterize oxidation chemistry (Donahue et al., 2011; Li et al., 2016). The VBS parameterization is
243 useful for classifying the wide range of OOMs into multiple volatility groups, including extremely low
244 volatility organic compounds (ELVOC) and low volatility organic compounds (LVOC) based on their
245 effective saturation concentration (C^*) in the unit of $\mu\text{g m}^{-3}$ (Bianchi et al., 2019). In this study, we
246 applied the VBS parameterization optimized by Li et al (Li et al., 2016; Isaacman-Vanwertz and
247 Aumont, 2021).

$$248 \log_{10}C^*(298K) = (n_C^0 - n_C)b_C - n_O b_O - 2 \frac{n_C n_O}{(n_C + n_O)} b_{CO} - n_N b_N - n_S b_S \quad (4)$$

249 where n_C , n_O , n_N , and n_S was the number of carbon, oxygen, nitrogen, and sulfur atoms of the
250 specific molecule, separately; n_C^0 was the reference carbon number; b_C , b_O , b_N , and b_S was the
251 contribution of each atom to $\log_{10}C^*$, respectively; b_{CO} was the carbon-oxygen nonideality (Donahue
252 et al., 2011). Values of b coefficient can be found in Li et al. (Li et al., 2016). The formula used to
253 estimate the vapor pressure was amended to convert all NO_3 groups into OH groups to reduce the bias
254 from the compounds containing nitrates (Daumit et al., 2013; Isaacman-Vanwertz and Aumont, 2021).

255 Due to the different temperatures in the CLOUD14 experiments, we adjusted $C^*(298K)$ to the
256 measured experimental temperature in equations (5) and (6):

$$257 \log_{10}C^*(T) = \log_{10}C^*(298K) + \frac{\Delta H_{vap}}{R \ln(10)} \times \left(\frac{1}{298} - \frac{1}{T} \right) \quad (5)$$

$$258 \Delta H_{vap}(\text{kJ mol}^{-1}) = -11 \cdot \log_{10}C^*(298K) + 129 \quad (6)$$

259 where T was the temperature in Kelvin, $C^*(298K)$ was the saturation vapor concentration at 298 K,
260 ΔH_{vap} was the evaporation enthalpy and R was the gas constant ($8.3134 \text{ J K}^{-1} \text{ mol}^{-1}$). The potential
261 presence of isomers may result in uncertainty in this method since the only input is the compound's
262 molecular formula.

263 In this study, all oxidation products were grouped into six volatility regimes; ultralow-volatility
264 (ULVOCs, $C^* < 10^{-8.5} \mu\text{g m}^{-3}$), extremely low volatility (ELVOCs, $10^{-8.5} < C^* < 10^{-4.5} \mu\text{g m}^{-3}$), low-
265 volatility (LVOCs, $10^{-4.5} < C^* < 10^{-0.5} \mu\text{g m}^{-3}$), semi-volatile (SVOCs, $10^{-0.5} < C^* < 10^{2.5} \mu\text{g m}^{-3}$),
266 intermediate-volatility organic compounds (IVOC, $10^{2.5} < C^* < 10^{6.5} \mu\text{g m}^{-3}$), and VOC ($10^{6.5} < C^* \mu\text{g}$
267 m^{-3}) based on VBS.

268 3 Results and Discussions

269 3.1 Peak identification of NH_4^+ -Orbitrap

270 As a promising reagent ion for detecting the full range of OOMs, more ions with low concentration
271 were captured by NH_4^+ , whose identification and quantification were most affected by overlapping
272 signals. The relative intensities of neighboring peaks should also be considered when estimating their
273 ease of separation. It has been shown that the higher mass resolution reduced the interference of
274 adjacent peaks based on NO_3^- or $\text{C}_2\text{H}_3\text{O}_2^-$ reagent ions (Riva et al., 2019a; Riva et al., 2020).
275 Therefore, the ability of the NH_4^+ -Orbitrap for separating overlapping mass spectral peaks was
276 compared to NH_4^+ -TOF.

277 The mass resolving power was defined as the ratio of m to Δm , where m was the mass-to-charge
278 ratio of the analyte ion, and Δm was the full width at half maximum (FWHM). Higher mass resolving
279 power allows unambiguous mass spectral peak assignment. For a pair of overlapping peaks of equal
280 intensity, the distance between their respective peak center, referred to hereafter simply as peak
281 distance, dm , needed to be greater than approximately 0.8 of the FWHM of the overlapping peaks,
282 such that they could be reasonably deconvolved as shown in Fig. S2. Depending on their experience,
283 individuals may be able to visually identify the presence of overlapping peaks at lower or higher dm
284 values. We arbitrarily defined the minimum dm (normalized to that of FWHM, or Δm) as the value at
285 which the observed spectrum (“Combined” trace in Fig. S2 and S3) had a local minimum between the
286 centers of the overlapping peaks (i.e., there was a “dip” in the observed signal between ion peaks). The
287 minimum dm value increased with the intensity ratio of overlapping peaks, ranging roughly from 0.85
288 (for equally intense peaks) to 1.43 (for peaks differing one order of magnitude in their respective
289 intensities), as shown in Fig. S3. In practice, noise and the presence of additional neighboring peaks
290 would further complicate peak deconvolution. For simplicity, we used a normalized dm of 1 (i.e., $dm =$
291 Δm) as a threshold for unambiguous deconvolution of neighboring peaks.

292 Figure 1 shows the histogram of the distances between neighboring peaks normalized against the
293 FWHM for the NH_4^+ -Orbitrap and the NH_4^+ -TOF having a mass resolving power of 10,000. In each
294 histogram, one count indicated that an ion had at least one neighboring ion with a relative intensity of
295 20%, 50%, or 100% (with a higher relative intensity threshold value being less selective). Neighboring
296 ions separated by distances exceeding 2 times the FWHM were considered well-separated. For ions
297 with multiple neighboring peaks within the 2 x FWHM separation distance window, the distance to the
298 first neighboring peak that satisfied the aforementioned relative intensity threshold was reported.
299 Overall, NH_4^+ -Orbitrap can separate most of the observed ions (> 99%), while the NH_4^+ -TOF,
300 depending on the relative intensity threshold set, can separate only 32% to 46% of all the ions by at
301 least 1 FWHM. **It should be noted that the NH_4^+ -Orbitrap has shown its strength in separating
302 neighboring peaks in controlled experiments, in which the knowledge of the chemical compositions
303 for OOMs is relatively abundant. The advantages of higher mass resolving power should be further
304 stressed in ambient observations, where the knowledge about OOM species can be limited with a
305 larger number of detectable peaks.**

306 3.2 Characterization of OOMs by four instruments

307 Illustrated in Fig. 2 are mass defect plots of OOMs measured by NH_4^+ -Orbitrap, NO_3^- -LTOF, PTR3-
308 TOF, and Γ^- -CIMS, identifying species of 484, 252, 145, and 67, respectively in run 2211. The NH_4^+ -
309 Orbitrap detected the widest range of products, including HOMs and the less oxidized species (i.e., O
310 < 6). Out of the 484 compounds, 5% were amines. The number of O atoms in OOMs varied from 1 to
311 11 in monomers (C_2 - C_{10}) and from 2 to 16 for dimeric products (C_{14} - C_{20}), with an average elemental
312 oxygen-to-carbon ratio (O:C) of 0.4 ± 0.2 . As expected, the NO_3^- -LTOF exhibited a very good
313 sensitivity towards HOMs, with the highest O:C of 0.7 ± 0.3 . The PTR3-TOF mainly detected
314 compounds below m/Q 300 Th with an average O:C of 0.5 ± 0.3 , which was due to the optimization to
315 (i.e., lowering E/N value) measure ammonia and amines sensitively, which ultimately impacted its
316 capability to detect efficiently OOMs. However, many less oxygenated OOMs were still observed by
317 the PTR3-TOF and were used to conduct the correlation analysis of time series with those detected by
318 the NH_4^+ -Orbitrap. Due to the selectivity and potential losses within the sampling line/inlet of the Γ^- -
319 CIMS equipped with a FIGAERO inlet fewer monomers of C_{8-10} and dimers of C_{19-20} were observed,
320 with an average O:C of 0.5 ± 0.2 .

321 **3.3 Instrumental comparisons: correlations**

322 Due to differences in selectivity and sensitivity of the analytical methods toward OOMs, ~42% of the
323 identified species by NH_4^+ -Orbitrap are simultaneously detected by other mass spectrometers (Fig.
324 S4). To identify how NH_4^+ -Orbitrap performed compared to the other mass spectrometers, a
325 correlation analysis including all co-detected ions was compiled. The experimental conditions of the
326 runs used for performing this analysis are summarized in Table S1. The data set covered a variety of
327 conditions, such as different concentrations of α -pinene, NO_x , SO_2 , and CO, as well as RH. R^2 was
328 calculated, using the time series of OOMs having the same elemental composition measured by the
329 different mass spectrometers. Figure 3 displays the correlation coefficient of time series for the
330 detected compounds, with marker size scaled by R^2 . The NH_4^+ -Orbitrap and the NO_3^- -LTOF detected
331 OOMs with the same chemical compositions, covering monomers and dimers, among which 18
332 OOMs showed $R^2 > 0.9$. Regarding the PTR3-TOF, the NH_4^+ -Orbitrap demonstrated high correlations
333 for most of the monomers and fewer dimers, including 32 species having an $R^2 > 0.9$. Due to potential
334 losses within the FIGAERO inlet, fewer OOMs were detected by the Γ^- -CIMS. However, certain
335 families of compounds, including $\text{C}_{10}\text{H}_{15}\text{O}_{5-7}\text{N}$ and $\text{C}_{20}\text{H}_{31}\text{O}_{7,9}\text{N}$ showed high correlations (i.e., $R^2 >$
336 0.9) between the NH_4^+ -Orbitrap and with the Γ^- -CIMS. Finally, the NO_3^- -LTOF was regarded as the
337 reference instrument for HOMs measurements. Only fewer monomers with high oxygen content were
338 detected by the NO_3^- -LTOF and the PTR3-TOF, and only a few dimers between the NO_3^- -LTOF and
339 the Γ^- -CIMS with moderate relevance. By comparing the coverage regions of the instruments across
340 multiple experimental conditions, the NH_4^+ -Orbitrap was capable of covering the widest range of
341 compounds and showed an overall good agreement with other mass spectrometers.

342 **3.4 Instrumental comparisons: concentration estimates**

343 Concentrations of the identified compounds were estimated for NH_4^+ -Orbitrap, as described in section
344 2.2. The sensitivity of NH_4^+ -Orbitrap was constrained using semi-quantitative information from the

345 other instruments. For instance, concentrations of the most abundant C₁₀-monomers (i.e., C₁₀H_{14/16}O_n)
346 were estimated using different calibration factors (Fig. 4), which were measured during steady-state
347 conditions (i.e., Run 2211 with [O₃] = 100 ppbv and [α-pinene] = 2 ppbv, RH = 10%). The
348 concentrations of C₁₀-monomers measured by the NH₄⁺-Orbitrap based on the two calibration factors
349 vary within a factor of 2, which indicates the consistency between the two correlation analyses. The
350 variation trend of concentrations with the oxygen number of the NH₄⁺-Orbitrap is similar to that of the
351 NO₃⁻-LTOF in the range of n_O>6, and it is similar to that of the PTR3-TOF in the range of n_O=1~5.
352 Taking into consideration that such ranges are also the oxygen number ranges with high sensitivities
353 respectively, this proves the robustness of the NH₄⁺-Orbitrap and the semi-quantification method. As
354 previously reported, the Orbitrap had a non-linear response to compounds present at extremely low
355 concentrations, which was independent of the sample composition, instrumental setup, or the reagent
356 ion (Riva et al., 2020; Cai et al., 2022). A similar evaluation was performed for the NH₄⁺-Orbitrap by
357 comparing the measured versus the theoretical isotopic intensities. As shown in Fig. S5, the NH₄⁺-
358 Orbitrap had a linear response for ion intensity greater than ~5 × 10³ cps, which corresponded to a
359 limit of quantification (LoQ, corresponding to the lowest normalized signal observed within the linear
360 range) of ~5 × 10⁵ molecules cm⁻³ for OOMs, estimated using the calibration factor derived from the
361 NO₃⁻-LTOF; which is consistent with a previous study (Riva et al., 2020).

362 Figure 5 presents the concentrations of all OOMs measured by the NH₄⁺-Orbitrap determined by
363 applying two different calibration factors. The concentrations of OOMs measured by the NH₄⁺-
364 Orbitrap were higher than both the NO₃⁻-LTOF and the PTR3-TOF which was optimized for
365 measuring ammonia and amines. This indicates that the NH₄⁺-Orbitrap can provide a better constraint
366 on the concentrations of the primary products. As an example, pinonaldehyde (i.e., C₁₀H₁₆O₂), as one
367 of the most abundant oxidation products, was not efficiently detected by the NO₃⁻-LTOF, which is
368 consistent with the higher selectivity of the NO₃⁻ reagent ion. To further illustrate the selectivity of the
369 different reagent ions, Fig. 6 offers a summary of the performance of each mass spectrometer in
370 detecting monomeric compounds, such as C₁₀H₁₆O_n. The y-axis is arbitrary and represents a qualitative
371 characterization of the oxygen content when compounds were detected by different CI schemes.
372 Similar to previous results, the I⁻-CIMS detected OOMs with n_O > 3, but was not optimal for the
373 detection of monomers with n_O > 7 (Riva et al., 2019b). The NO₃⁻-LTOF was mainly selective
374 towards HOMs with n_O > 6 (Riva et al., 2019b). The PTR3-TOF had limited capabilities in detecting
375 OOMs with n_O > 5 due to the optimization of the instrument to obtain a very sensitive measurement of
376 ammonia. Previously, the amine-CI demonstrated promise for the detection of OOMs, but was limited
377 to applications with comparatively clean conditions due to considerable depletion of the reagent ion
378 and the presence of overlapping peaks (Berndt et al., 2018b; Riva et al., 2019b). While showing a
379 similar OOMs detection range to amine-CI, NH₄⁺-CI in tandem with the greater mass resolving power
380 of the Orbitrap mass analyzer provided a linear response to higher loading. As shown in Fig. S6,
381 background peaks were not affected by atmospherically relevant concentrations of O₃ and α-pinene.
382 Overall, the NH₄⁺-Orbitrap appears to have the potential for providing a more reliable

383 identification/quantification of OOMs produced from VOC oxidation compared to other existing mass
384 spectrometry techniques.

385 **3.5 Volatility distribution by four instruments**

386 Figure 7 shows the distribution of oxidation products measured by four MS instruments according to
387 their saturation vapor concentrations ($\log_{10}C_{\text{sat}}$) estimated using the modified Li et al. approach (Li et
388 al., 2016; Isaacman-Vanwertz and Aumont, 2021). OOMs were grouped into six volatility regimes
389 based on a volatility basis set (VBS): ultra-low volatility (ULVOCs); extremely low volatility
390 (ELVOCs); low-volatility (LVOCs); semi-volatile (SVOCs); intermediate volatility organic
391 compounds (IVOC); and VOC. ULVOCs and ELVOCs initiate cluster growth and form new particles.
392 The total signal in each volatility bin represented the sum of the signal intensity of OOMs within the
393 volatility range. The mean contributions of these compound regimes are shown in the VBS pie charts.
394 The ULVOC, ELVOC, and LVOC regimes were well captured by NH_4^+ -Orbitrap and NO_3^- -LTOF.
395 The PTR3-TOF only characterized the SVOC and IVOC regime (along with VOCs). IVOC and VOC
396 regimes in the PTR3-TOF and NH_4^+ -Orbitrap were generally less oxygenated VOCs (i.e., $n_{\text{O}} < 5$).
397 IVOC comprised the biggest mass contributions for the NH_4^+ -Orbitrap, and LVOC dominated in the
398 NO_3^- -LTOF. Hence, the detection of the NH_4^+ -Orbitrap covered the widest range of volatilities,
399 clearly highlighting the benefit of using this technique for the formation and fate of OOMs. In the past,
400 reagent switching has not been practical, and users would run multiple mass spectrometer systems in
401 parallel or use a Multi-scheme chemical IONization inlet (MION) with only one mass spectrometer to
402 obtain the fullest possible mass spectrum (Rissanen et al., 2019; Huang et al., 2021). With NH_4^+ -
403 Orbitrap it is now possible to cover the entire range of compounds which was not the case with most
404 CI techniques.

405 **3.6 RH dependence of NH_4^+ -Orbitrap**

406 The sensitivity of the reagent-adduct ionization has been reported to be affected by the presence of
407 water vapor for a variety of reagent ions (Lee et al., 2014; Breitenlechner et al., 2017). The impact of
408 RH on the detection of OOMs by the NH_4^+ -Orbitrap was also studied. While the concentrations of gas
409 phase precursor and oxidant remained constant, the RH was raised from 10% to 80%. During this
410 increase the signal of organic vapor behaved inconsistently under an otherwise constant gas-phase
411 production rate (Surdu et al., 2023) and an increase in the condensation sink (Fig. S7). As shown in
412 Fig. 8, the NH_4^+ -Orbitrap demonstrated an RH dependence. For instance, the signal of less oxygenated
413 molecules (i.e., $n_{\text{O}} < 5$) increased with increasing RH, especially compounds with $n_{\text{C}} = 8$; while the
414 signal of highly oxygenated molecules (i.e., $n_{\text{O}} > 10$) decreased as a function of RH. The average
415 behavior of all C_{8-10} monomers and C_{18-20} dimers was summarized and compared between four
416 instruments (Fig. S8). The other three mass spectrometers also showed obvious RH dependence.
417 Similar to NH_4^+ -Orbitrap, OOMs with $n_{\text{O}} < 5$ measured by NO_3^- -LTOF and PTR3-TOF increased at
418 high RH, and a reverse tendency for HOMs with $n_{\text{O}} > 11$, while OOMs with $n_{\text{O}} = 8\sim 11$ seemed to be
419 independent to RH. The large variations of OOMs intensity at different RH measured by NH_4^+ -
420 Orbitrap may be due to the widest range of oxygen atoms. The causes why OOMs with different

421 oxygen numbers measured by four instruments changed with RH was not clear. Here, multiple
422 possible reasons were provided to explain the signal evolution of the ions with changing RH, such as
423 water affecting the ionization efficiency or altering the physicochemical processes of the gas phase
424 chemistry.

425 First, the efficiency of a particular compound partly relied on whether water vapor competes with
426 the ammonium ion, lowering the sensitivity, or whether it acted as a third body to stabilize the
427 ammonium-organic analyte cluster by removing extra energy from the collision, raising the sensitivity
428 (Lee et al., 2014). NH_4^+ primary ions can cluster with water molecules when humidity increased,
429 thereby reducing the clustering of the NH_4^+ with organic analytes (Breitenlechner et al., 2017).
430 However, the formed NH_4^+X_n (X being NH_3 or H_2O ; $n = 1,2$) clusters might also act as reagent ions
431 and ionize OOMs through ligand switching reactions, which were expected to be fast and thus
432 improve the charging efficiency (Hansel et al., 2018). Compared to previous NH_4^+ -CIMS, the NH_4^+X_n
433 reagent ions were expected to be larger due to the absence of the field in the ion-molecular-reaction
434 zone in Orbitrap, resulting in greater ligand exchanging and increasing the sensitivity for the less
435 oxygenated species (Canaval et al., 2019).

436 For RH-independent compounds, this may be due to the existence of very stable complexes with
437 NH_4^+ reagent ion, or sufficient internal vibrational modes to disperse extra energy from the collision
438 (Lee et al., 2014). The highly oxygenated dimers in the category of ULVOCs and ELVOCs which
439 largely partition to the particle phase regardless of the presence of water might indicate that water may
440 also affect the physicochemical processes (i.e., multiphase chemistry, partitioning, etc.), in this case
441 possibly leading to an increase in the driving force of gas-particle partitioning of highly oxygenated
442 species (Surdu et al., 2023), and/or causing the decomposition of highly oxygenated molecules in the
443 particle phase to create less and moderately oxygenated products, e.g., $\text{C}_8\text{H}_{12}\text{O}_{1-5}$ (up to a 30-fold
444 increase in the gas phase) (Pospisilova et al., 2020), although which in the range of SVOCs (e.g.,
445 $\text{C}_8\text{H}_{12}\text{O}_{4,5}$) was also thought to partition more to the particle phase at higher RH (Surdu et al., 2023).
446 Finally, while water vapor could affect the gas-phase chemistry through water reactions with the
447 Criegee intermediates (CIs), HO_2 chemistry, OH radical concentration, no clear evidence has been
448 identified as earlier discussed by Surdu et al (2023). However, the accurate reasons needs to be further
449 verified in target control experiments like changing the RH in IMR of CI inlet.

450 **4 Summary**

451 In conclusion, this study presented an intercomparison between NH_4^+ -Orbitrap, NO_3^- -LTOF, PTR3-
452 TOF, and I^- -CIMS based on the identification and quantification of OOMs formed from the ozonolysis
453 of α -pinene under various environmental conditions. We used NH_4^+ adduct ions with the Orbitrap
454 mass spectrometer to measure the oxygenated species for the first time. NH_4^+ -Orbitrap is a promising
455 CIMS technique for a comprehensive measurement of the whole product distribution and provides a
456 more complete understanding of the molecular composition and volatility of OOMs. This allows
457 NH_4^+ -Orbitrap to better monitor the evolution of organic compounds, which can be beneficial for air
458 quality, pollutant transport, and climate models. It is worth expecting that NH_4^+ -Orbitrap can be not

459 only useful for laboratory-based studies but also to field observations, to provide a deeper
460 understanding of atmospheric oxidation processes. However, it remains challenging to accurately
461 quantify the concentrations of OOMs due to the absent signals of reagent ions. In addition, RH
462 influences NH_4^+ -Orbitrap sensitivity, which can be different for each OOM. Therefore, this specific
463 effect requires more attention and dedicated studies before that the NH_4^+ -Orbitrap can be used in field
464 studies, for example, injection of pure or mixture of standards in atmospheric chamber at varying RH.
465 From what is presented here, the understanding of RH effect on the NH_4^+ -Orbitrap capabilities is too
466 scarce to be able to understand the time series evolution of OOMs that would be obtained in the real
467 atmosphere.

468 **Conflicts of interest**

469 There are no conflicts to declare.

470 **Acknowledgements**

471 We thank the European Organization for Nuclear Research (CERN) for supporting CLOUD with
472 important technical and financial resources. We thank the Orbitool team for developing the tools to
473 analyze mass spectra. This work was financially supported by the French National program LEFE
474 (Les Enveloppes Fluides et l'Environnement), the European Research Council (ERC-StG MAARvEL;
475 no. 852161), the European Union's Horizon 2020 research and innovation programme (Marie
476 Sklodowska-Curie grant agreement no. 764991 and 701647), the Swiss National Science Foundation
477 (no. 200021_169090, 200020_172602, 20FI20_172622, and 206021_198140), the US National
478 Science Foundation (NSF_AGS_1801280, NSF_AGC_1801574, NSF_AGS_1801897,
479 NSF_AGS_2132089), and the German Federal Ministry of Education and Research (CLOUD-16
480 01LK1601A). D.D.L. thanks the China Scholarship Council of P. R. China for the Ph.D. grant.
481 M.Y.W. acknowledges financial support from the Schmidt Science Fellows Program by Schmidt
482 Futures, in partnership with the Rhodes Trust.

483 **Author Contributions**

484 D.D.L., D.Y.W., L.C., W.S., M.Y.W., S.T., G.M., M.S., E.E., X.D.G., L.G.-C., M.G., J.P., B.R., B.S.,
485 P.R., S.P., A.H., J.C., J.K., N.M.D., C.G., I.E.-H., and M.R. prepared the CLOUD facility or
486 measuring instruments. D.D.L., D.Y.W., L.C., W.S., M.Y.W., S.T., G.M., M.S., E.E., X.D.G., L.G.-
487 C., M.G., J.P., B.R., B.S., J.K., and M.R. collected the CLOUD data. D.D.L., D.Y.W., L.C., W.S.,
488 M.Y.W., G.M., and M.R. analysed the data. D.D.L., D.Y.W., M.Y.W., N.M.D., C.G., I.E.-H., and
489 M.R. wrote the manuscript and contributed to the scientific discussion. All authors discussed the
490 results and commented on the paper.

491 **References**

492 Berndt, T., Mentler, B., Scholz, W., Fischer, L., Herrmann, H., Kulmala, M., and Hansel, A.:
493 Accretion Product Formation from Ozonolysis and OH Radical Reaction of α -Pinene: Mechanistic
494 Insight and the Influence of Isoprene and Ethylene, *Environmental Science & Technology*, 52, 11069-
495 11077, 10.1021/acs.est.8b02210, 2018a.

496 Berndt, T., Scholz, W., Mentler, B., Fischer, L., Herrmann, H., Kulmala, M., and Hansel, A.:
497 Accretion Product Formation from Self- and Cross-Reactions of RO₂ Radicals in the Atmosphere,
498 *Angewandte Chemie International Edition*, 57, 3820-3824, 10.1002/anie.201710989, 2018b.

499 Bianchi, F., Kurten, T., Riva, M., Mohr, C., Rissanen, M. P., Roldin, P., Berndt, T., Crouse, J. D.,
500 Wennberg, P. O., Mentel, T. F., Wildt, J., Junninen, H., Jokinen, T., Kulmala, M., Worsnop, D. R.,
501 Thornton, J. A., Donahue, N., Kjaergaard, H. G., and Ehn, M.: Highly Oxygenated Organic Molecules
502 (HOM) from Gas-Phase Autoxidation Involving Peroxy Radicals: A Key Contributor to Atmospheric
503 Aerosol, *Chemical reviews*, 119, 3472-3509, 10.1021/acs.chemrev.8b00395, 2019.

504 Bianchi, F., Tröstl, J., Junninen, H., Frege, C., Henne, S., Hoyle, C. R., Molteni, U., Herrmann, E.,
505 Adamov, A., Bukowiecki, N., Chen, X., Duplissy, J., Gysel, M., Hutterli, M., Kangasluoma, J.,
506 Kontkanen, J., Kürten, A., Manninen, H. E., Münch, S., Peräkylä, O., Petäjä, T., Rondo, L.,
507 Williamson, C., Weingartner, E., Curtius, J., Worsnop, D. R., Kulmala, M., Dommen, J., and
508 Baltensperger, U.: New particle formation in the free troposphere: A question of chemistry and timing,
509 *Science*, 352, 1109-1112, 10.1126/science.aad5456, 2016.

510 Breitenlechner, M., Fischer, L., Hainer, M., Heinritzi, M., Curtius, J., and Hansel, A.: PTR3: An
511 Instrument for Studying the Lifecycle of Reactive Organic Carbon in the Atmosphere, *Analytical*
512 *Chemistry*, 89, 5824-5831, 10.1021/acs.analchem.6b05110, 2017.

513 Cai, R., Huang, W., Meder, M., Bourgain, F., Aizikov, K., Riva, M., Bianchi, F., and Ehn, M.:
514 Improving the Sensitivity of Fourier Transform Mass Spectrometer (Orbitrap) for Online
515 Measurements of Atmospheric Vapors, *Analytical chemistry*, 94, 15746-15753,
516 10.1021/acs.analchem.2c03403, 2022.

517 Cai, R., Li, Y., Clément, Y., Li, D., Dubois, C., Fabre, M., Besson, L., Perrier, S., George, C., Ehn,
518 M., Huang, C., Yi, P., Ma, Y., and Riva, M.: Orbitool: a software tool for analyzing online Orbitrap
519 mass spectrometry data, *Atmospheric Measurement Techniques*, 14, 2377-2387, 10.5194/amt-14-
520 2377-2021, 2021.

521 Canaval, E., Hyttinen, N., Schmidbauer, B., Fischer, L., and Hansel, A.: NH₄⁺ Association and Proton
522 Transfer Reactions With a Series of Organic Molecules, *Frontiers in Chemistry*, 7,
523 10.3389/fchem.2019.00191, 2019.

524 Caudillo, L., Rörup, B., Heinritzi, M., Marie, G., Simon, M., Wagner, A. C., Müller, T., Granzin, M.,
525 Amorim, A., Ataci, F., Baalbaki, R., Bertozzi, B., Brasseur, Z., Chiu, R., Chu, B., Dada, L., Duplissy,
526 J., Finkenzeller, H., Gonzalez Carracedo, L., He, X. C., Hofbauer, V., Kong, W., Lamkaddam, H.,
527 Lee, C. P., Lopez, B., Mahfouz, N. G. A., Makhmutov, V., Manninen, H. E., Marten, R., Massabò, D.,
528 Mauldin, R. L., Mentler, B., Molteni, U., Onnela, A., Pfeifer, J., Philippov, M., Piedehierro, A. A.,
529 Schervish, M., Scholz, W., Schulze, B., Shen, J., Stolzenburg, D., Stozhkov, Y., Surdu, M., Tauber,
530 C., Tham, Y. J., Tian, P., Tomé, A., Vogt, S., Wang, M., Wang, D. S., Weber, S. K., Welti, A.,
531 Yonghong, W., Yusheng, W., Zauner-Wieczorek, M., Baltensperger, U., El Haddad, I., Flagan, R. C.,
532 Hansel, A., Höhler, K., Kirkby, J., Kulmala, M., Lehtipalo, K., Möhler, O., Saathoff, H., Volkamer,

533 R., Winkler, P. M., Donahue, N. M., Kürten, A., and Curtius, J.: Chemical composition of
534 nanoparticles from α -pinene nucleation and the influence of isoprene and relative humidity at low
535 temperature, *Atmospheric Chemistry and Physics*, 21, 17099-17114, 10.5194/acp-21-17099-2021,
536 2021.

537 Daumit, K. E., Kessler, S. H., and Kroll, J. H.: Average chemical properties and potential formation
538 pathways of highly oxidized organic aerosol, *Faraday discussions*, 165, 181-202, 10.1039/c3fd00045a,
539 2013.

540 Donahue, N. M., Epstein, S. A., Pandis, S. N., and Robinson, A. L.: A two-dimensional volatility basis
541 set: 1. organic-aerosol mixing thermodynamics, *Atmospheric Chemistry and Physics*, 11, 3303-3318,
542 10.5194/acp-11-3303-2011, 2011.

543 Ehn, M., Junninen, H., Petäjä, T., Kurtén, T., Kerminen, V. M., Schobesberger, S., Manninen, H. E.,
544 Ortega, I. K., Vehkamäki, H., Kulmala, M., and Worsnop, D. R.: Composition and temporal behavior
545 of ambient ions in the boreal forest, *Atmospheric Chemistry and Physics*, 10, 8513-8530, 10.5194/acp-
546 10-8513-2010, 2010.

547 Ehn, M., Thornton, J. A., Kleist, E., Sipila, M., Junninen, H., Pullinen, I., Springer, M., Rubach, F.,
548 Tillmann, R., Lee, B., Lopez-Hilfiker, F., Andres, S., Acir, I. H., Rissanen, M., Jokinen, T.,
549 Schobesberger, S., Kangasluoma, J., Kontkanen, J., Nieminen, T., Kurten, T., Nielsen, L. B.,
550 Jorgensen, S., Kjaergaard, H. G., Canagaratna, M., Maso, M. D., Berndt, T., Petaja, T., Wahner, A.,
551 Kerminen, V. M., Kulmala, M., Worsnop, D. R., Wildt, J., and Mentel, T. F.: A large source of low-
552 volatility secondary organic aerosol, *Nature*, 506, 476-479, 10.1038/nature13032, 2014.

553 Fan, J., Wang, Y., Rosenfeld, D., and Liu, X.: Review of Aerosol–Cloud Interactions: Mechanisms,
554 Significance, and Challenges, *Journal of the Atmospheric Sciences*, 73, 4221-4252, 10.1175/jas-d-16-
555 0037.1, 2016.

556 Hallquist, M., Wenger, J. C., Baltensperger, U., Rudich, Y., Simpson, D., Claeys, M., Dommen, J.,
557 Donahue, N. M., George, C., Goldstein, A. H., Hamilton, J. F., Herrmann, H., Hoffmann, T., Iinuma,
558 Y., Jang, M., Jenkin, M. E., Jimenez, J. L., Kiendler-Scharr, A., Maenhaut, W., McFiggans, G.,
559 Mentel, T. F., Monod, A., Prévôt, A. S. H., Seinfeld, J. H., Surratt, J. D., Szmigielski, R., and Wildt,
560 J.: The formation, properties and impact of secondary organic aerosol: current and emerging issues,
561 *Atmospheric Chemistry and Physics*, 9, 5155-5236, 10.5194/acp-9-5155-2009, 2009.

562 Hansel, A., Scholz, W., Mentler, B., Fischer, L., and Berndt, T.: Detection of RO₂ radicals and other
563 products from cyclohexene ozonolysis with NH₄⁺ and acetate chemical ionization mass spectrometry,
564 *Atmospheric Environment*, 186, 248-255, 10.1016/j.atmosenv.2018.04.023, 2018.

565 Haywood, J. and Boucher, O.: Estimates of the direct and indirect radiative forcing due to tropospheric
566 aerosols: A review, *Reviews of Geophysics*, 38, 513-543, 10.1029/1999rg000078, 2000.

567 Heinritzi, M., Simon, M., Steiner, G., Wagner, A. C., Kürten, A., Hansel, A., and Curtius, J.:
568 Characterization of the mass-dependent transmission efficiency of a CIMS, Atmospheric
569 Measurement Techniques, 9, 1449-1460, 10.5194/amt-9-1449-2016, 2016.

570 Huang, W., Li, H., Sarnela, N., Heikkinen, L., Tham, Y. J., Mikkilä, J., Thomas, S. J., Donahue, N.
571 M., Kulmala, M., and Bianchi, F.: Measurement report: Molecular composition and volatility of
572 gaseous organic compounds in a boreal forest – from volatile organic compounds to highly
573 oxygenated organic molecules, Atmospheric Chemistry and Physics, 21, 8961-8977, 10.5194/acp-21-
574 8961-2021, 2021.

575 Isaacman-VanWertz, G. and Aumont, B.: Impact of organic molecular structure on the estimation of
576 atmospherically relevant physicochemical parameters, Atmospheric Chemistry and Physics, 21, 6541-
577 6563, 10.5194/acp-21-6541-2021, 2021.

578 Jimenez, J. L., Canagaratna, M. R., Donahue, N. M., Prevot, A. S. H., Zhang, Q., Kroll, J. H.,
579 DeCarlo, P. F., Allan, J. D., Coe, H., Ng, N. L., Aiken, A. C., Docherty, K. S., Ulbrich, I. M.,
580 Grieshop, A. P., Robinson, A. L., Duplissy, J., Smith, J. D., Wilson, K. R., Lanz, V. A., Hueglin, C.,
581 Sun, Y. L., Tian, J., Laaksonen, A., Raatikainen, T., Rautiainen, J., Vaattovaara, P., Ehn, M., Kulmala,
582 M., Tomlinson, J. M., Collins, D. R., Cubison, M. J., Dunlea, J., Huffman, J. A., Onasch, T. B.,
583 Alfarra, M. R., Williams, P. I., Bower, K., Kondo, Y., Schneider, J., Drewnick, F., Borrmann, S.,
584 Weimer, S., Demerjian, K., Salcedo, D., Cottrell, L., Griffin, R., Takami, A., Miyoshi, T.,
585 Hatakeyama, S., Shimojo, A., Sun, J. Y., Zhang, Y. M., Dzepina, K., Kimmel, J. R., Sueper, D.,
586 Jayne, J. T., Herndon, S. C., Trimborn, A. M., Williams, L. R., Wood, E. C., Middlebrook, A. M.,
587 Kolb, C. E., Baltensperger, U., and Worsnop, D. R.: Evolution of Organic Aerosols in the
588 Atmosphere, *Science*, 326, 1525-1529, doi:10.1126/science.1180353, 2009.

589 Jokinen, T., Sipilä, M., Junninen, H., Ehn, M., Lönn, G., Hakala, J., Petäjä, T., Mauldin, R. L.,
590 Kulmala, M., and Worsnop, D. R.: Atmospheric sulphuric acid and neutral cluster measurements using
591 CI-API-TOF, Atmospheric Chemistry and Physics, 12, 4117-4125, 10.5194/acp-12-4117-2012, 2012.

592 Kirkby, J., Duplissy, J., Sengupta, K., Frege, C., Gordon, H., Williamson, C., Heinritzi, M., Simon,
593 M., Yan, C., Almeida, J., Tröstl, J., Nieminen, T., Ortega, I. K., Wagner, R., Adamov, A., Amorim,
594 A., Bernhammer, A.-K., Bianchi, F., Breitenlechner, M., Brilke, S., Chen, X., Craven, J., Dias, A.,
595 Ehrhart, S., Flagan, R. C., Franchin, A., Fuchs, C., Guida, R., Hakala, J., Hoyle, C. R., Jokinen, T.,
596 Junninen, H., Kangasluoma, J., Kim, J., Krapf, M., Kürten, A., Laaksonen, A., Lehtipalo, K.,
597 Makhmutov, V., Mathot, S., Molteni, U., Onnela, A., Peräkylä, O., Piel, F., Petäjä, T., Praplan, A. P.,
598 Pringle, K., Rap, A., Richards, N. A. D., Riipinen, I., Rissanen, M. P., Rondo, L., Sarnela, N.,
599 Schobesberger, S., Scott, C. E., Seinfeld, J. H., Sipilä, M., Steiner, G., Stozhkov, Y., Stratmann, F.,
600 Tomé, A., Virtanen, A., Vogel, A. L., Wagner, A. C., Wagner, P. E., Weingartner, E., Wimmer, D.,
601 Winkler, P. M., Ye, P., Zhang, X., Hansel, A., Dommen, J., Donahue, N. M., Worsnop, D. R.,
602 Baltensperger, U., Kulmala, M., Carslaw, K. S., and Curtius, J.: Ion-induced nucleation of pure
603 biogenic particles, *Nature*, 533, 521, 10.1038/nature17953, 2016.

604 Lee, B. H., Lopez-Hilfiker, F. D., Mohr, C., Kurtén, T., Worsnop, D. R., and Thornton, J. A.: An
605 Iodide-Adduct High-Resolution Time-of-Flight Chemical-Ionization Mass Spectrometer: Application
606 to Atmospheric Inorganic and Organic Compounds, *Environmental Science & Technology*, 48, 6309-
607 6317, 10.1021/es500362a, 2014.

608 Li, H., Almeida, T. G., Luo, Y., Zhao, J., Palm, B. B., Daub, C. D., Huang, W., Mohr, C., Krechmer,
609 J. E., Kurtén, T., and Ehn, M.: Fragmentation inside proton-transfer-reaction-based mass
610 spectrometers limits the detection of ROOR and ROOH peroxides, *Atmospheric Measurement
611 Techniques*, 15, 1811-1827, 10.5194/amt-15-1811-2022, 2022.

612 Li, Y., Pöschl, U., and Shiraiwa, M.: Molecular corridors and parameterizations of volatility in the
613 chemical evolution of organic aerosols, *Atmospheric Chemistry and Physics*, 16, 3327-3344,
614 10.5194/acp-16-3327-2016, 2016.

615 Lopez-Hilfiker, F. D., Mohr, C., Ehn, M., Rubach, F., Kleist, E., Wildt, J., Mentel, T. F., Lutz, A.,
616 Hallquist, M., Worsnop, D., and Thornton, J. A.: A novel method for online analysis of gas and
617 particle composition: description and evaluation of a Filter Inlet for Gases and AEROSols
618 (FIGAERO), *Atmospheric Measurement Techniques*, 7, 983-1001, 10.5194/amt-7-983-2014, 2014.

619 Mellouki, A., Wallington, T. J., and Chen, J.: Atmospheric chemistry of oxygenated volatile organic
620 compounds: impacts on air quality and climate, *Chemical reviews*, 115, 3984-4014,
621 10.1021/cr500549n, 2015.

622 Mohr, C., Thornton, J. A., Heitto, A., Lopez-Hilfiker, F. D., Lutz, A., Riipinen, I., Hong, J., Donahue,
623 N. M., Hallquist, M., Petäjä, T., Kulmala, M., and Yli-Juuti, T.: Molecular identification of organic
624 vapors driving atmospheric nanoparticle growth, *Nature Communications*, 10, 10.1038/s41467-019-
625 12473-2, 2019.

626 Pospisilova, V., Lopez-Hilfiker, F. D., Bell, D. M., El Haddad, I., Mohr, C., Huang, W., Heikkinen,
627 L., Xiao, M., Dommen, J., Prevot, A. S. H., Baltensperger, U., and Slowik, J. G.: On the fate of
628 oxygenated organic molecules in atmospheric aerosol particles, *Science Advances*, 6, eaax8922,
629 doi:10.1126/sciadv.aax8922, 2020.

630 Rissanen, M. P., Mikkilä, J., Iyer, S., and Hakala, J.: Multi-scheme chemical ionization inlet (MION)
631 for fast switching of reagent ion chemistry in atmospheric pressure chemical ionization mass
632 spectrometry (CIMS) applications, *Atmospheric Measurement Techniques*, 12, 6635-6646,
633 10.5194/amt-12-6635-2019, 2019.

634 Riva, M., Brüggemann, M., Li, D., Perrier, S., George, C., Herrmann, H., and Berndt, T.: Capability of
635 CI-Orbitrap for Gas-Phase Analysis in Atmospheric Chemistry: A Comparison with the CI-API-TOF
636 Technique, *Analytical Chemistry*, 92, 8142-8150, 10.1021/acs.analchem.0c00111, 2020.

637 Riva, M., Ehn, M., Li, D., Tomaz, S., Bourgain, F., Perrier, S., and George, C.: CI-Orbitrap: An
638 Analytical Instrument To Study Atmospheric Reactive Organic Species, *Analytical Chemistry*, 91,
639 9419-9423, 10.1021/acs.analchem.9b02093, 2019a.

640 Riva, M., Rantala, P., Krechmer, J. E., Peräkylä, O., Zhang, Y., Heikkinen, L., Garmash, O., Yan, C.,
641 Kulmala, M., Worsnop, D., and Ehn, M.: Evaluating the performance of five different chemical
642 ionization techniques for detecting gaseous oxygenated organic species, *Atmospheric Measurement*
643 *Techniques*, 12, 2403-2421, 10.5194/amt-12-2403-2019, 2019b.

644 Schobesberger, S., Junninen, H., Bianchi, F., Lonn, G., Ehn, M., Lehtipalo, K., Dommen, J., Ehrhart,
645 S., Ortega, I. K., Franchin, A., Nieminen, T., Riccobono, F., Hutterli, M., Duplissy, J., Almeida, J.,
646 Amorim, A., Breitenlechner, M., Downard, A. J., Dunne, E. M., Flagan, R. C., Kajos, M., Keskinen,
647 H., Kirkby, J., Kupc, A., Kurten, A., Kurten, T., Laaksonen, A., Mathot, S., Onnela, A., Praplan, A. P.,
648 Rondo, L., Santos, F. D., Schallhart, S., Schnitzhofer, R., Sipila, M., Tome, A., Tsagkogeorgas, G.,
649 Vehkamäki, H., Wimmer, D., Baltensperger, U., Carslaw, K. S., Curtius, J., Hansel, A., Petaja, T.,
650 Kulmala, M., Donahue, N. M., and Worsnop, D. R.: Molecular understanding of atmospheric particle
651 formation from sulfuric acid and large oxidized organic molecules, *Proceedings of the National*
652 *Academy of Sciences of the United States of America*, 110, 17223-17228, 10.1073/pnas.1306973110,
653 2013.

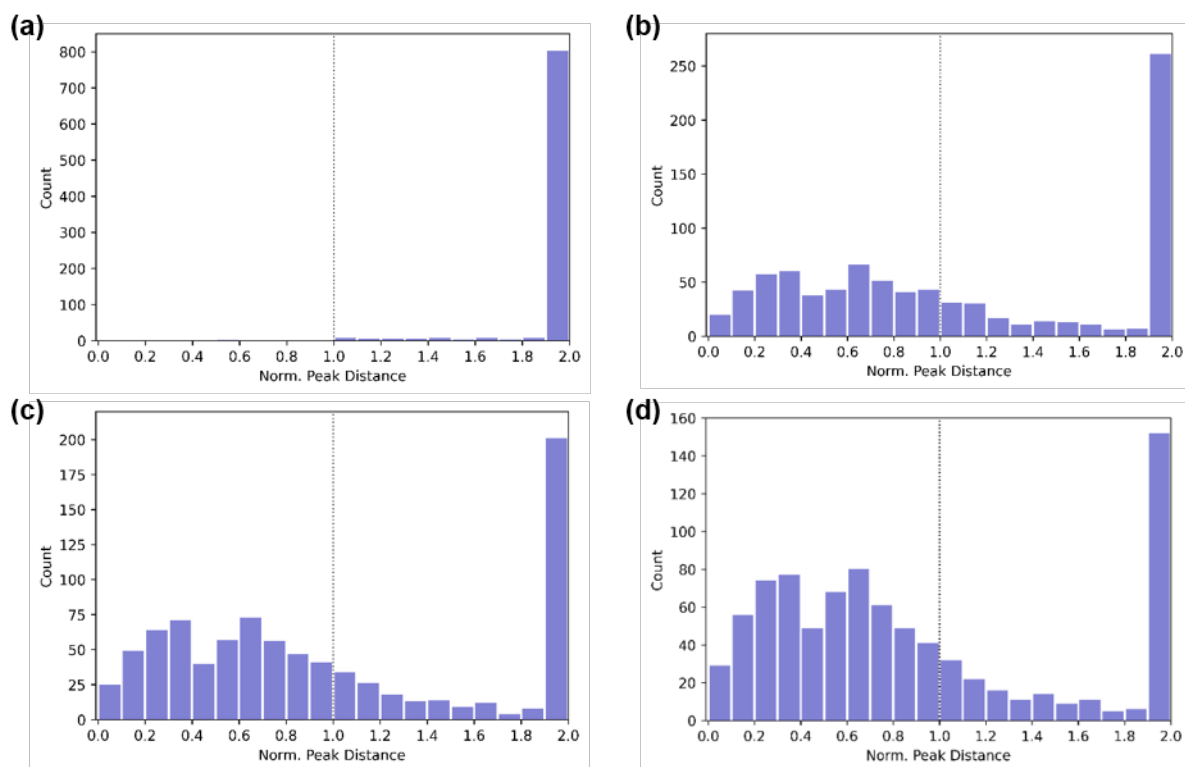
654 Simon, M., Dada, L., Heinritzi, M., Scholz, W., Stolzenburg, D., Fischer, L., Wagner, A. C., Kürten,
655 A., Rörup, B., He, X.-C., Almeida, J., Baalbaki, R., Baccarini, A., Bauer, P. S., Beck, L., Bergen, A.,
656 Bianchi, F., Bräkling, S., Brilke, S., Caudillo, L., Chen, D., Chu, B., Dias, A., Draper, D. C., Duplissy,
657 J., El-Haddad, I., Finkenzeller, H., Frege, C., Gonzalez-Carracedo, L., Gordon, H., Granzin, M.,
658 Hakala, J., Hofbauer, V., Hoyle, C. R., Kim, C., Kong, W., Lamkaddam, H., Lee, C. P., Lehtipalo, K.,
659 Leiminger, M., Mai, H., Manninen, H. E., Marie, G., Marten, R., Mentler, B., Molteni, U., Nichman,
660 L., Nie, W., Ojdanic, A., Onnela, A., Partoll, E., Petäjä, T., Pfeifer, J., Philippov, M., Quéléver, L. L.
661 J., Ranjithkumar, A., Rissanen, M. P., Schallhart, S., Schobesberger, S., Schuchmann, S., Shen, J.,
662 Sipilä, M., Steiner, G., Stozhkov, Y., Tauber, C., Tham, Y. J., Tomé, A. R., Vazquez-Pufleau, M.,
663 Vogel, A. L., Wagner, R., Wang, M., Wang, D. S., Wang, Y., Weber, S. K., Wu, Y., Xiao, M., Yan,
664 C., Ye, P., Ye, Q., Zauner-Wieczorek, M., Zhou, X., Baltensperger, U., Dommen, J., Flagan, R. C.,
665 Hansel, A., Kulmala, M., Volkamer, R., Winkler, P. M., Worsnop, D. R., Donahue, N. M., Kirkby, J.,
666 and Curtius, J.: Molecular understanding of new-particle formation from α -pinene between -50 and
667 $+25$ °C, *Atmospheric Chemistry and Physics*, 20, 9183-9207, 10.5194/acp-20-9183-2020, 2020.

668 Stolzenburg, D., Fischer, L., Vogel, A. L., Heinritzi, M., Schervish, M., Simon, M., Wagner, A. C.,
669 Dada, L., Ahonen, L. R., Amorim, A., Baccarini, A., Bauer, P. S., Baumgartner, B., Bergen, A.,
670 Bianchi, F., Breitenlechner, M., Brilke, S., Buenrostro Mazon, S., Chen, D., Dias, A., Draper, D. C.,
671 Duplissy, J., El Haddad, I., Finkenzeller, H., Frege, C., Fuchs, C., Garmash, O., Gordon, H., He, X.,
672 Helm, J., Hofbauer, V., Hoyle, C. R., Kim, C., Kirkby, J., Kontkanen, J., Kürten, A., Lampilahti, J.,
673 Lawler, M., Lehtipalo, K., Leiminger, M., Mai, H., Mathot, S., Mentler, B., Molteni, U., Nie, W.,
674 Nieminen, T., Nowak, J. B., Ojdanic, A., Onnela, A., Passananti, M., Petäjä, T., Quéléver, L. L. J.,
675 Rissanen, M. P., Sarnela, N., Schallhart, S., Tauber, C., Tomé, A., Wagner, R., Wang, M., Weitz, L.,
676 Wimmer, D., Xiao, M., Yan, C., Ye, P., Zha, Q., Baltensperger, U., Curtius, J., Dommen, J., Flagan,
677 R. C., Kulmala, M., Smith, J. N., Worsnop, D. R., Hansel, A., Donahue, N. M., and Winkler, P. M.:
678 Rapid growth of organic aerosol nanoparticles over a wide tropospheric temperature range,
679 *Proceedings of the National Academy of Sciences*, 115, 9122-9127, 10.1073/pnas.1807604115, 2018.

680 Surdu, M., Lamkaddam, H., Wang, D. S., Bell, D. M., Xiao, M., Lee, C. P., Li, D., Caudillo, L.,
681 Marie, G., Scholz, W., Wang, M., Lopez, B., Piedehierro, A. A., Ataei, F., Baalbaki, R., Bertozzi, B.,
682 Bogert, P., Brasseur, Z., Dada, L., Duplissy, J., Finkenzeller, H., He, X.-C., Höhler, K., Korhonen, K.,
683 Krechmer, J. E., Lehtipalo, K., Mahfouz, N. G. A., Manninen, H. E., Marten, R., Massabò, D.,
684 Mauldin, R., Petäjä, T., Pfeifer, J., Philippov, M., Rörup, B., Simon, M., Shen, J., Umo, N. S., Vogel,
685 F., Weber, S. K., Zauner-Wieczorek, M., Volkamer, R., Saathoff, H., Möhler, O., Kirkby, J., Worsnop,
686 D. R., Kulmala, M., Stratmann, F., Hansel, A., Curtius, J., Welti, A., Riva, M., Donahue, N. M.,
687 Baltensperger, U., and El Haddad, I.: Molecular Understanding of the Enhancement in Organic
688 Aerosol Mass at High Relative Humidity, *Environmental Science & Technology*, 57, 2297-2309,
689 10.1021/acs.est.2c04587, 2023.

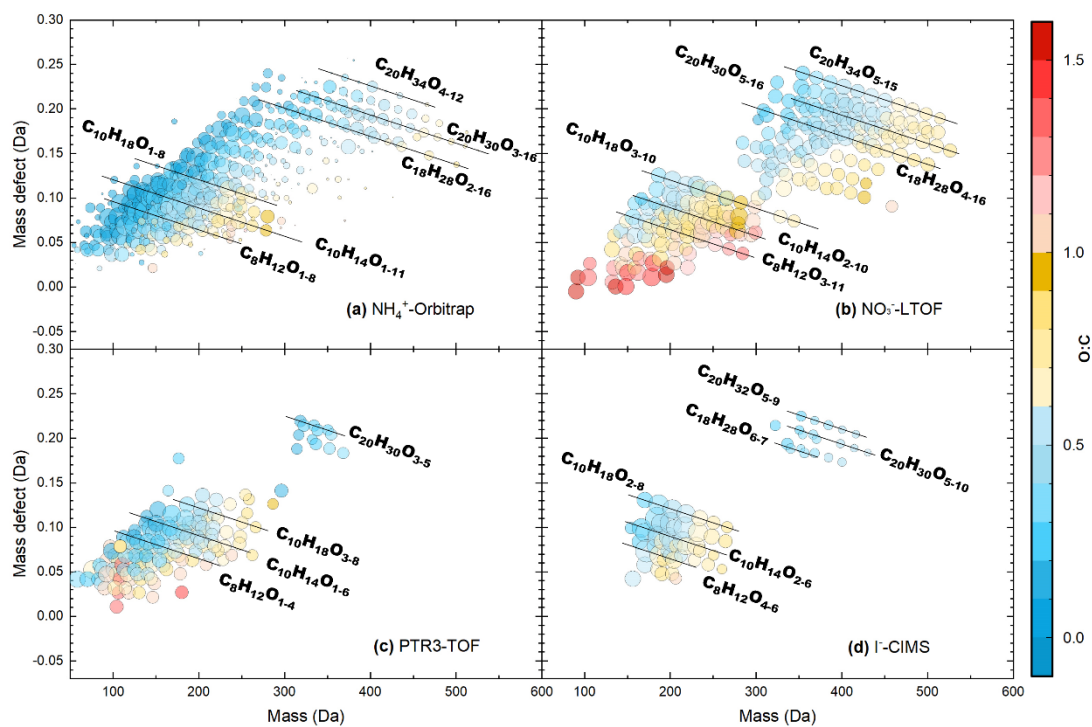
690 Wang, M., Kong, W., Marten, R., He, X.-C., Chen, D., Pfeifer, J., Heitto, A., Kontkanen, J., Dada, L.,
691 Kürten, A., Yli-Juuti, T., Manninen, H. E., Amanatidis, S., Amorim, A., Baalbaki, R., Baccarini, A.,
692 Bell, D. M., Bertozzi, B., Bräkling, S., Brilke, S., Murillo, L. C., Chiu, R., Chu, B., De Menezes, L.-P.,
693 Duplissy, J., Finkenzeller, H., Carracedo, L. G., Granzin, M., Guida, R., Hansel, A., Hofbauer, V.,
694 Krechmer, J., Lehtipalo, K., Lamkaddam, H., Lampimäki, M., Lee, C. P., Makhmutov, V., Marie, G.,
695 Mathot, S., Mauldin, R. L., Mentler, B., Müller, T., Onnela, A., Partoll, E., Petäjä, T., Philippov, M.,
696 Pospisilova, V., Ranjithkumar, A., Rissanen, M., Rörup, B., Scholz, W., Shen, J., Simon, M., Sipilä,
697 M., Steiner, G., Stolzenburg, D., Tham, Y. J., Tomé, A., Wagner, A. C., Wang, D. S., Wang, Y.,
698 Weber, S. K., Winkler, P. M., Wlasits, P. J., Wu, Y., Xiao, M., Ye, Q., Zauner-Wieczorek, M., Zhou,
699 X., Volkamer, R., Riipinen, I., Dommen, J., Curtius, J., Baltensperger, U., Kulmala, M., Worsnop, D.
700 R., Kirkby, J., Seinfeld, J. H., El-Haddad, I., Flagan, R. C., and Donahue, N. M.: Rapid growth of new
701 atmospheric particles by nitric acid and ammonia condensation, *Nature*, 581, 184-189,
702 10.1038/s41586-020-2270-4, 2020.

703



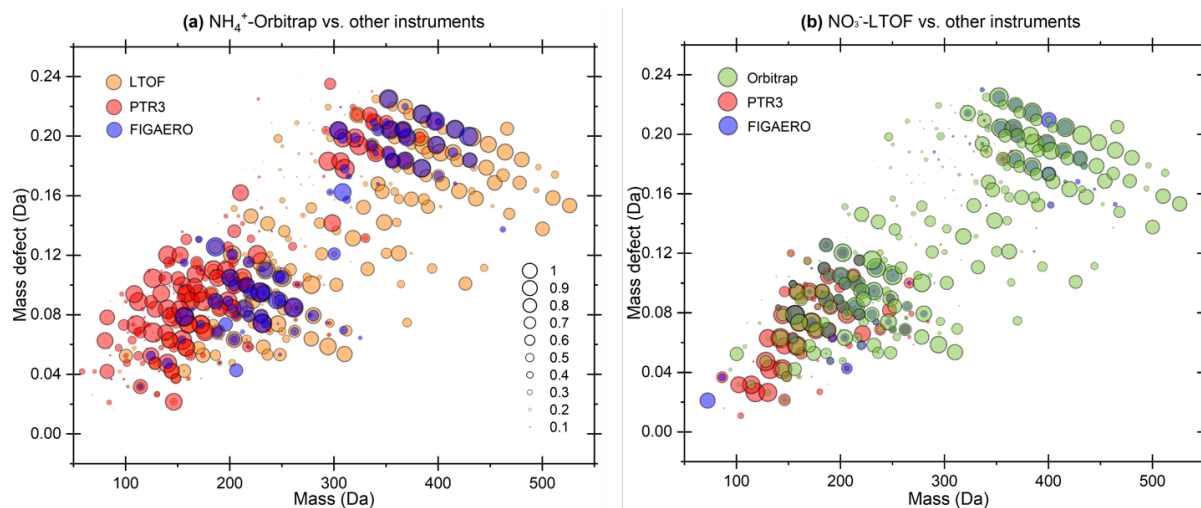
704

705 **Figure 1:** Number of adjacent peaks within a intensity threshold as the function of normalized peak
 706 distance observed by (a) NH_4^+ -Orbitrap and (b, c, d) NH_4^+ -TOF, respectively. The normalized peak
 707 distance was the ratio of distance between neighboring peaks to the full width at half maximum
 708 (FWHM). For each ion, the distance to the closest neighbor with a relative peak intensity that
 709 exceeded 20%, 50%, or 100% is recorded. (a) Orbitrap mass analyzer >99% of ions were separated by
 710 at least 1 FWHM from their neighbors with relative intensity threshold being set at 20%. (b) TOF
 711 mass analyzer (mass resolution $\sim 10,000$) >46% of ions were separated by at least 1 FWHM from their
 712 neighbors with a relative intensity threshold being set at 100%. (c) TOF mass analyzer >39% of ions
 713 were separated by at least 1 FWHM from their neighbors with a relative intensity threshold being set
 714 at 50%. (d) TOF mass analyzer >32% of ions were separated by at least 1 FWHM from their
 715 neighbors with a relative intensity threshold being set at 20%.



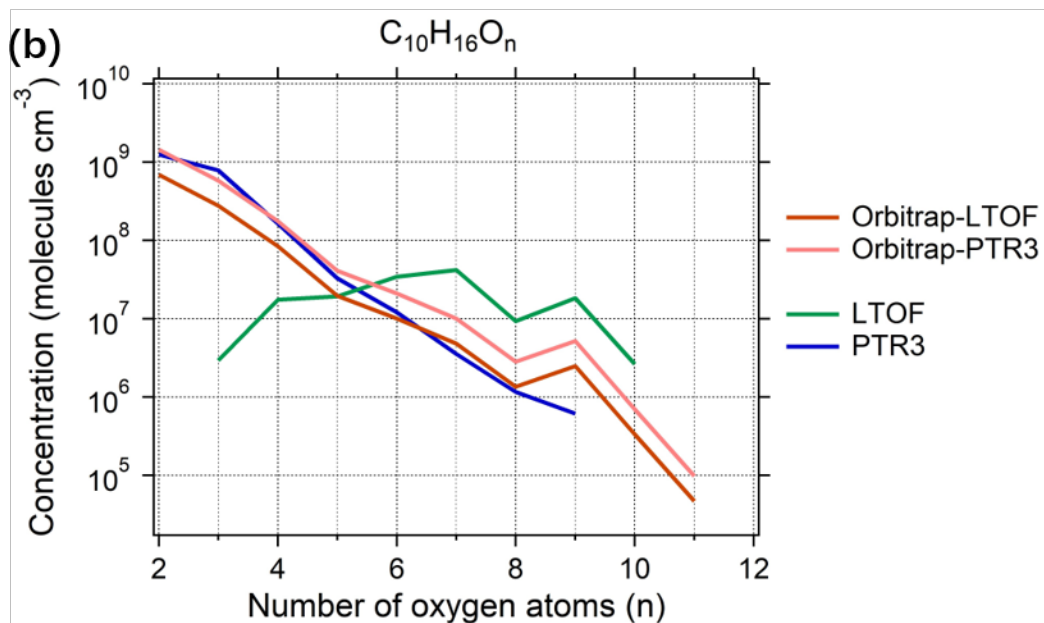
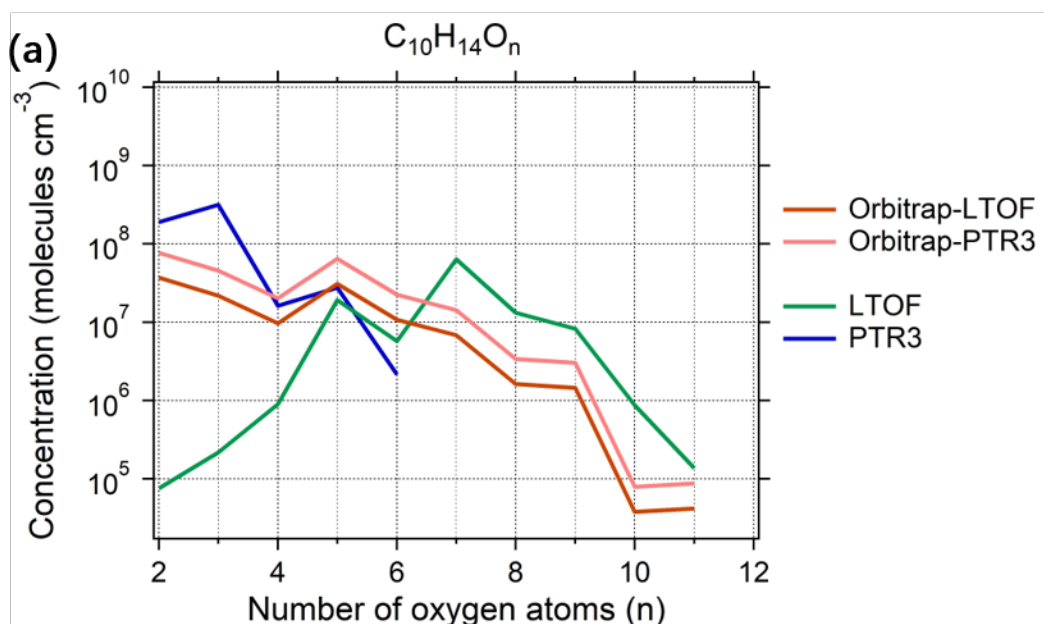
716

717 **Figure 2:** Mass defect plots for organic compounds measured by (a) NH_4^+ -Orbitrap, (b) NO_3^- -LTOF,
 718 (c) PTR3-TOF and (d) I-CIMS in run 2211. The x-axis represents the mass-to-charge ratio of the
 719 neutral analyte and the y-axis represents the corresponding mass defect, which is the difference
 720 between their exact mass and nominal mass (Schobesberger et al., 2013). Markers were all sized by
 721 the logarithm of their corresponding signals and colored by the O:C value. Some major OOMs
 722 measured by different instruments were indicated by the black lines.



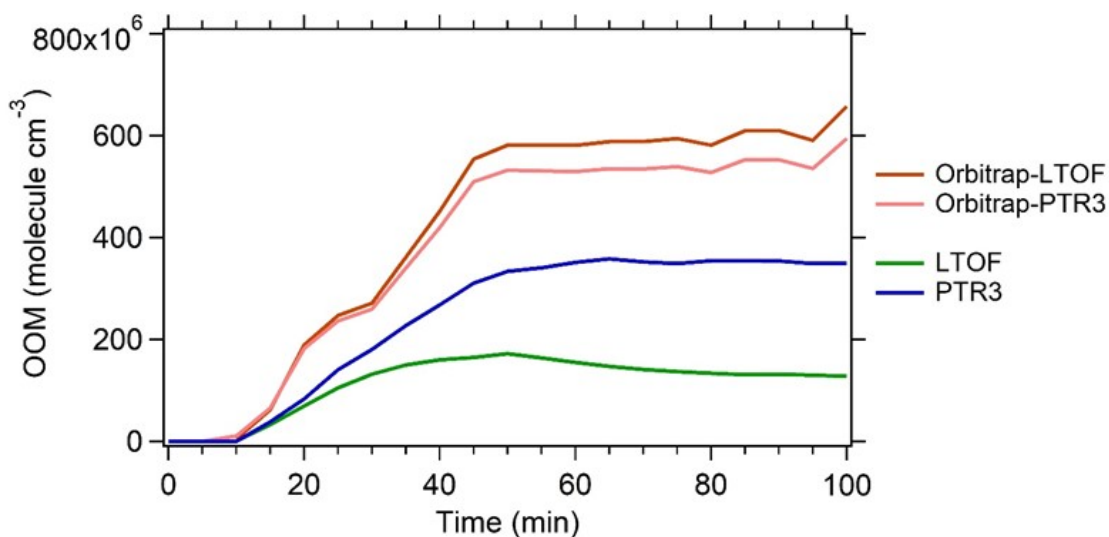
723

724 **Figure 3:** Mass defect plots depicting the compounds of which time series correlation was observed
 725 by (a) NH₄⁺-Orbitrap and (b) NO₃⁻-LTOF with other MS instruments. Each circle represents a
 726 molecule and marker size represents the correlation R² of time series of the molecules between two
 727 different MS instruments. Two sets of data in run 2211 and 2213 were used to reduce uncertainties.



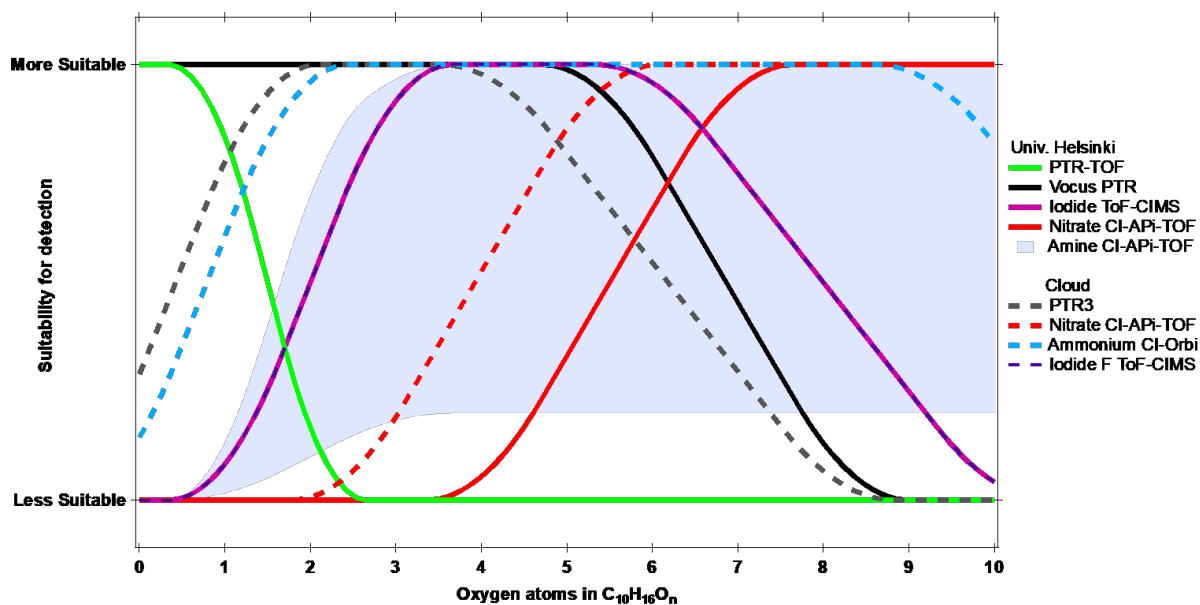
728

729 **Figure 4:** Estimated concentrations of the main C_{10} oxidation products (a) $C_{10}H_{14}O_n$ and (b) $C_{10}H_{16}O_n$
 730 as a function of oxygen numbers observed in run 2211. Orbitrap-LTOF and Orbitrap-PTR3
 731 represented the estimated concentration of monomers measured by NH_4^+ -Orbitrap using the
 732 calibration factors from the correlation analysis with NO_3^- -LTOF and PTR3-TOF, respectively.



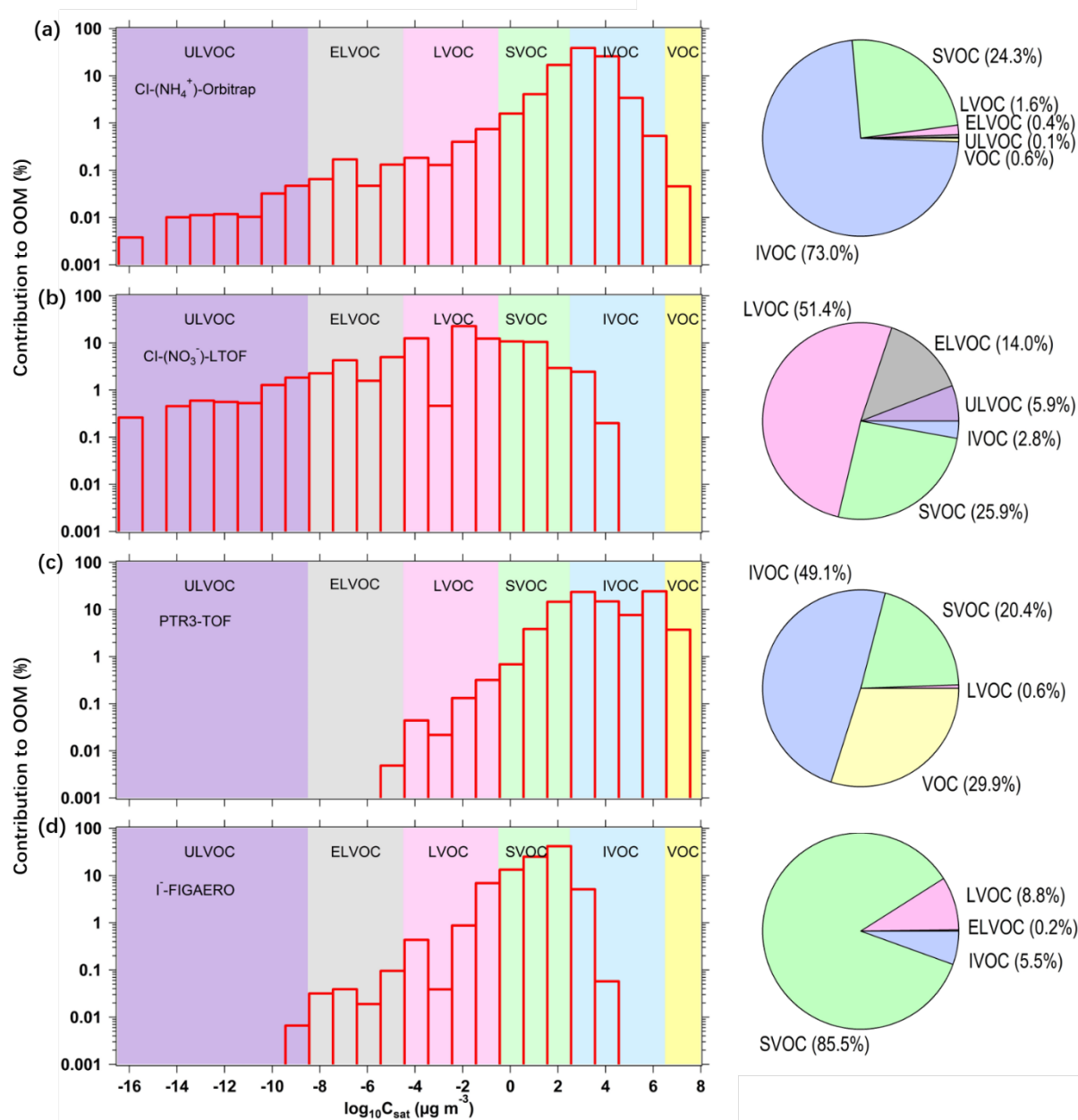
733

734 **Figure 5:** Estimated concentrations of all measured OOMs in the photooxidation of α -pinene. All
 735 monomers C_{8-10} and dimers C_{18-20} measured by NH_4^+ -Orbitrap, NO_3^- -LTOF, and PTR3-TOF in run
 736 2213 were summed up. The concentrations of OOMs measured by NH_4^+ -Orbitrap were quantified by
 737 the calibration factors derived from correlation analysis between NH_4^+ -Orbitrap and NO_3^- -LTOF
 738 (Orbitrap-LTOF, light green) or PTR3-TOF (Orbitrap-PTR3, light blue), respectively.



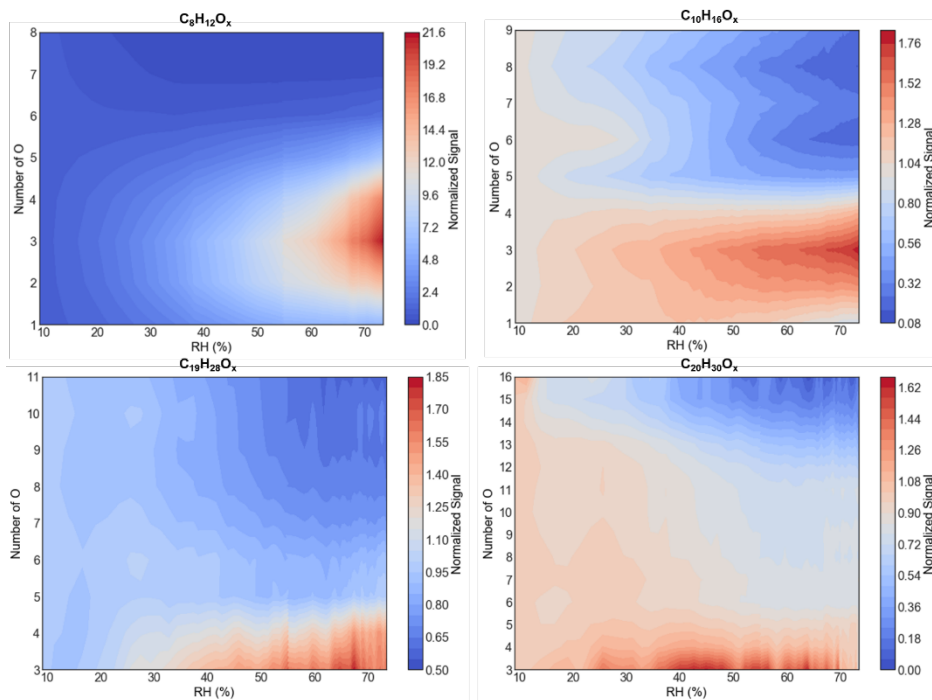
739

740 **Figure 6:** Estimated detection suitability of the different CIMS techniques for monomers from α -
 741 pinene ozonolysis, plotted as a function of the number of oxygen atoms. Image modified from Riva et
 742 al.(Riva et al., 2019b).



743

744 **Figure 7:** Volatility distribution comparison for organic compounds detected by (a) NH_4^+ -Orbitrap,
 745 (b) NO_3^- -LTOF, (c) PTR3-TOF and (d) I^- -CIMS. The background colors represent the saturation
 746 concentration (C_{sat}) in the range of ultra-low volatility (ULVOCs, purple), extremely low volatility
 747 (ELVOCs, gray), low volatility (LVOCs, pink), semi-volatile (SVOCs, green), intermediate volatility
 748 (IVOCs, blue) and volatile organic compounds (VOCs). The right pie charts are the corresponding
 749 contributions of VOC, IVOC, SVOC, LVOC, ELVOC, and ULVOC classes in run 2211.
 750 Concentrations were used to calculate the contribution in each volatility bin for NO_3^- -LTOF and
 751 PTR3-TOF, while signals were calculated for NH_4^+ -Orbitrap and I^- -CIMS.



752

753 **Figure 8:** The effect of relative humidity on the distribution of the most abundant monomers and
 754 dimers measured by NH_4^+ -Orbitrap. The RH ramped from $\sim 10\%$ to $\sim 80\%$ in run 2211. The normalized
 755 signal represents the signal variation ratio at certain RH compared to that at $\text{RH} = 10\%$, normalized

756
$$\text{signal} = \frac{\text{signal}_{RH}}{\text{signal}_{10\%}}.$$